

Optical and X-ray Observational Search for the Possible Supernova Remnant Candidates in the Nearby Galaxy NGC 1569

E. N. Ercan,¹★ E. Aktekin,¹ N. Cesur² and A. Tümer¹

¹Department of Physics, Bogazici University, 34342, Istanbul, Turkey

²Department of Physics, Yıldız Technical University, 34220, Istanbul, Turkey

Accepted XXX. Received YYY; in original form ZZZ

ABSTRACT

We report the results of our investigation on the possible existence of supernova remnants (SNRs) in the nearby galaxy, NGC 1569, using the CCD imaging and spectroscopic observations from the RTT150 telescope of TUG-TUBITAK in Antalya, Turkey for two different observing periods. Using $[\text{S II}]/\text{H}\alpha \geq 0.4$ standard criteria, the identification of 13 new SNR candidates for this galaxy is proposed for two different epochs. We found the $[\text{S II}]/\text{H}\alpha$ ratios ranging from 0.46–0.84 and $\text{H}\alpha$ intensities ranging from $(2.2\text{--}32) \times 10^{-15} \text{ erg cm}^{-2} \text{ s}^{-1}$. $[\text{S II}]\lambda\lambda 6716/6731$ average flux ratio is calculated from the optical spectra for only one possible SNR candidate. By using this ratio the electron density, N_e , is estimated to be $121 \pm 17 \text{ cm}^{-3}$ and by using the $[\text{O III}]\lambda 5007/\text{H}\beta$ ratio of the same spectrum, the shock wave velocity, V_s , is estimated to be between $100 < V_s < 150 \text{ km s}^{-1}$. Using *Chandra* data, we find that out of 13 SNR candidates only 10 of them have yielded a spectrum with good statistics, confirming the existence of 10 SNR candidates with matched positions in X-ray region as well. We measure the 0.5–2 keV band flux down to $0.58 \times 10^{-15} \text{ erg cm}^{-2} \text{ s}^{-1}$ for 10 X-ray sources. Our spectral analysis revealed that spectra of the SNR candidates are best modelled with the Collisional Ionisation Equilibrium plasma with a temperature range of $0.84 \text{ keV} < kT_e < 1.36 \text{ keV}$.

Key words: galaxies: individual NGC 1569, galaxies: star formation - ISM: supernova remnants - X-rays: galaxies - X-rays: ISM

1 INTRODUCTION

The optical, X-ray and radio investigations of extragalactic supernova remnants (SNRs) can be used to understand the evolution of SNRs, to estimate the supernovae rate and SNRs population in galaxies, and to study the global properties of the interstellar medium and environments in the galaxy (see e.g. Matonick & Fesen 1997; Panuti et al. 2000; Sonbaş et al. 2010; Lee & Lee 2014).

Strong ratio of $[\text{S II}]$ with respect to $\text{H}\alpha$ line of SNRs are great indicators of this nebula emission which also has an extended X-ray along with powerful non-thermal radio emission (Long 1985). In order to identify SNRs, investigation has to be performed by the utilization of tools such as narrow band imaging with $\text{H}\alpha$ and $[\text{S II}]$ filters, radio observations, and X-ray imaging.

NGC 1569 is a nearby dwarf irregular and a well-known

starburst galaxy found in the Camelopardalis constellation, which was discovered by William Herschel in 1788. With an apparent visual magnitude of 11.9, NGC 1569 lies at a distance of 11 million light years, i.e. 3.4 Mpc (Lelli, Verheijen & Fraternali 2014; Jackson, Hunter & Oh 2011; Kobulnicky & Skillman 1997).

Grocholski et al. (2008) have presented deep Hubble Space Telescope (HST) Advanced Camera for Surveys / Wide Field Channel (ACS/WFC) results and determined the distance to be $3.36 \pm 0.20 \text{ Mpc}$ which is considerably farther away than its previously observed value of only $2.2 \pm 0.6 \text{ Mpc}$ by Israel (1988). It is part of the group as IC 342 group of galaxies, which was initially assumed to be an isolated galaxy due to its underestimated distance. Its high density character reveals NGC 1569's starburst nature, which in general is the result of galaxy interactions. In addition, as opposed to what was originally thought, this galaxy contains higher numbers of starbursts implied by their extended spread. Early predictions for star formation rates for

★ E-mail: ercan@boun.edu.tr (NE)

stars younger than 1 Gyr enhanced the evidence by a factor of more than two, while older stars were not subjected to such restrictions.

Another work done in optical for the intrinsic extinction distribution of NGC 1569, [Relano et al. \(2006a\)](#), reported the use of an optical extinction map (A_V) obtained from their $H\alpha/H\beta$ emission line ratio for this purpose, and they obtained values up to $A_V = 0.8$ mag.

[Devost, Roy & Drissen \(1997\)](#) reported deep $H\alpha$ imaging and multi-slit optical spectroscopy results of 16 H II regions. The optical extinction for NGC 1569 was obtained from the Balmer $H\alpha/H\beta$ line ratio emphasizing the fact that most of the observed A_V was caused by Milky Way emission, which gave (A_V) local = 1.61 ± 0.09 . However, the intrinsic A_V for NGC 1569 was found to be 0.65 ± 0.04 .

[Chomiuk & Wilcots \(2009\)](#) reported their survey for 4 nearby irregular galaxies for SNR candidates in the radio region including NGC 1569, by using deep ($1\sigma \sim 20\mu\text{Jy}$) high resolution (~ 20 pc) VLA continuum data at 20, 6, and 3.6 cm. They identified discrete sources and categorized them as SNRs, H II regions, or background radio galaxies with the use of radio spectral indices and $H\alpha$ images. Their classifications were found to be consistent with the early studies. According to their results NGC 1569 contains 23 SNR candidates.

[Della Ceca et al. \(1996\)](#) have studied the X-ray aspects of dwarf starburst inside NGC 1569, using their *ASCA* observations along with archival data from *ROSAT* PSPC and HRI, $H\alpha$ images of optical broad and narrow bands, combined with recent IR K-band images. Soft and hard components were discovered from the *ASCA* SIS broad-band X-ray spectrum (0.5–6 keV). Thermal model fitting of the soft component provided the temperature values ranging from ~ 0.64 – 0.8 keV, whereas ~ 3.7 keV thermal model or 2.1 photon index of power-law component individually fitted the hard component. Extended X-ray emission was observed in the soft component and its morphology was associated with $H\alpha$ filaments.

It is generally believed that X-ray observations may provide strong evidence that starbursts can drive gas out of the dwarf galaxies, as it was seen from the diffuse X-ray emission analysis of NGC 1569. The X-ray data can establish the diffuse X-ray emission in NGC 1569 produced by hot gas and also can tell us that the temperature of this gas may exceed the depth of the galaxy’s shallow potential well.

[Jürgen, Fabian & Elias \(2005\)](#) also found an extended diffuse X-ray emission which was associated with temperatures ranged from 1.6 to 7.6×10^6 K from *Chandra* X-ray observations.

The most recent optical and X-ray observations of NGC 1569 have been reported by [Sánchez-Cruces et al. \(2015\)](#) describing the optical lines of $H\alpha$ and $[\text{S II}]\lambda\lambda 6716, 6731 \text{ \AA}$. They achieved their optical observations in $H\alpha$ and $[\text{S II}]$ conducted with the UNAM scanning FabryPerot interferometer (PUMA) and the X-ray data obtained from the *Chandra* data archive. They observed several superbubbles, filaments, and supershells in NGC 1569 for which they determined their sizes as well as their kinematical properties. In their *Chandra* observation result also a total of 54 possible X-ray emission coordinates were recorded in their Table 9. Amongst 54 of them they listed a possible description of their characteristic types that could be considered as active

Table 1. Physical properties of NGC 1569.

Parameters	Value	References
Other Names	UGC03056, ARP210, VII Zw 016	(1)
Morphological Type	IBm	(1)
Position (J2000)	RA(J2000) : $04^{\text{h}}30^{\text{m}}47^{\text{s}}.48$ Dec. (J2000): $64^{\circ}50'55''.70$	
Visual Magnitude	11.9	(2)
Distance	3.4 Mpc	(2)
Diameter	1.69 kpc	(3)

References: (1) NASA Extragalactic Database, (2) ([Lelli, Verheijen & Fraternali 2014](#); [Jackson, Hunter & Oh 2011](#); [Kobulnicky & Skillman 1997](#)), (3) [Sánchez-Cruces et al. \(2015\)](#).

galactic nuclei, X-ray sources, X-ray binaries, stars and two possible SNRs.

The main physical properties of NGC 1569 retrieved from aforementioned studies are summarised in Table 1.

We have particular interest in performing a systematic study to search for possible SNR candidates in nearby galaxies and we started with NGC 1569 for which we had long exposure times in optical in two different epochs as well as the X-ray archival data of *Chandra* (see Section 2 for both) to be able to achieve our aim. This work will present the first optical study for NGC 1569 using the data of RTT150 at TUG.

Some of the possible SNR candidates have already been observed in optical region by us earlier (NGC 1569 was one of them) but the limited observing times did not let us present our results with poor time statistics then. However, even with short time observations we have noticed and detected some SNR candidates in our preliminary results (including so-called No.1 observations, in this text) but preferred to wait for another chance of getting a better and longer observing time to observe NGC 1569 again with RTT150.

In fact, we finally achieved this with No.1 and a longer No.2 observations. As we have mentioned in the text during the No.1. (spectral) observations, we had only one chance of getting the spectrum of one of the SNR candidate out of a total of 13 SNR candidates for NGC 1569 because of the limited observing conditions. Having much longer observing period during the second epoch of our observations, we were then able to present both of our observation in a total "combined" observational optical data obtained from the addition of No.1 and and No.2 as shown in Table 2.

2 OBSERVATIONS AND DATA REDUCTION

Our optical observations are performed in two different periods of observing time of RTT150¹ approximately seven months apart from each other. So called-No.1 is done on the 28 & 29th March 2017 and No.2 is on the 25th December 2017.

We have combined our so-called No.1 and No.2 observations as one single long exposure optical observation by RTT150. One can see the CCD configurations of our observations through the link

¹ Specifications of RTT150 and TFOSC are available at <http://www.tug.tubitak.gov.tr>.

provided at the TUG Observatory internet page : <http://tug.tubitak.gov.tr/en/teleskoplar/rtt150-0>.

2.1 Optical Imaging Observations

The optical imaging observations of NGC 1569 took place on the 29th March 2017 (No.1 observation) and 25th December 2017 (No.2 observation) with the 1.5 m RTT150 in Antalya, Turkey and images are obtained with the low-resolution TUG Faint Object Spectrograph and Camera (TFOSC). It is equipped with a 2048 × 2048 back-illuminated camera. For the No.1 observations, a pixel size of 15 μm corresponding to a 13.5 arcmin square field of view (FoV), and for the No.2 observations, a pixel size of 13.5 μm was used giving a 11.5 arcmin square FoV attached to the Cassegrain focus of the RTT150. Narrow-band filters centered lines of [S II], Hα, and continuum filters were used. The interference filter characteristics and our exposure times of imaging observations are shown in Table 2.

Eventually Image Reduction and Analysis Facility (IRAF) was used to reduce the combined optical data. Data reduction was achieved by using standard procedures, including the corrections for bias, overscan at field, and removal of cosmic rays using the IRAF CCDPROC package. Hα and [S II] images were subtracted from Hα and [S II] continuum. Using *imarith* package of IRAF, continuum subtraction and image division were realised. *Imarith* package which subtracts and divides the number of photons in each pixel of the obtained image. Each night the spectrophotometric standard star Feige 34 from Massey et al. (1988) was observed for the flux calibration. Jacoby, Africano & Quigley (1987) described the conversion from instrumental counts in to physical units (erg cm⁻² s⁻¹). We used *Combine* package of IRAF to combine No.1 and No.2 observations. ([S II] - [S II] continuum) / (Hα - Hα continuum) combined images were obtained, then compared with the theoretical models which generally predict [S II]/Hα ratios to be in the range of 0.5–1.0 for SNR candidates (see e.g. Raymond 1979; Shull & Mckee 1979). A total of 13 SNR candidates near the central part of the NGC 1569 with appropriate [S II]/Hα values are reported as shown in Table 3 (see in Fig. 1).

2.2 Optical Spectral Analysis

The optical spectral observations were performed on the 28th of March 2017 with RTT150. High-resolution long-slit spectra of one out of 13 SNR candidates located at RA(J2000) = 04^h30^m48^s.42, Dec. (J2000) = 64°50′53″.60 were obtained with the low-resolution TFOSC. Spectral analysis for only one of the SNR candidates is reported here, because of the limited seeing conditions of the telescope for the rest of the candidates.

During the observations, grism 15 with a dispersion of 8 Å (λ3230–9120 Å) was used. The slit width was 134 micron. Fe-Ar calibration lamp frames were obtained for slit width for each observation. The exposure time was 900 sec for the frame. The data reduction (the data and lamp were bias-corrected with a median bias frame, and divided by a normalised field), wavelength and flux calibrations were carried out by using the standard IRAF routines. The signal to noise ratio was calculated to be 15 at [O III]λ 5007

Å line. The signal to noise ratio was found to be low (as low as ~2; longward of 7500 Å) since grism 15 with a dispersion of 8 Å (3230–9120 Å) was used during our observations; so we had to cut the spectrum after 7500 Å. Optical spectrum of SNR candidate ID5 (RA(J2000) = 04^h30^m48^s.42, Dec. (J2000) = 64°50′53″.60) at a range of λ 3500–7500 Å is shown in Fig. 2.

[S II]/Hα was calculated and the electron density was obtained through [S II](λ6716/λ6731) flux ratio as described by (Osterbrock & Ferland 2006). Regarding using [O III]λ5007/Hβ line ratio diagnostics to estimate the shock velocities, V_s, associated with extragalactic SNRs, one can follow the standard works done by Matonick & Fesen (1997) and the earlier discussions and calculations of [O III]λ5007/Hβ ratios done by Dopita et al. (1984) in which they used fully-radiative plane-parallel shock models to estimate the [O III]λ5007/Hβ ratio (among other elemental ratios) as a function of shock velocity. In Dopita et al. (1984) study their Figs.5 & 6, show the plots of this ratio as a function of shock velocity. Our [O III]λ5007/Hβ ratio value of 4.5 obtained from our spectral analysis for SNR candidate ID 5 gives us an estimate of 100 < V_s < 150 km s⁻¹. The interstellar extinction and the extinction of Hα produced by such a dust screen distribution are also determined through the relations of Relano et al. (2006b); Buat et al. (2002):

$$A_{(H\alpha)} = 5.25 \times \log[(H\alpha/H\beta)/(2.859 \times t_e^{-0.07})] \quad (1)$$

$$E(B - V) = 0.44/2.45 \times A_{(H\alpha)} \quad (2)$$

where Hα/Hβ stands for the observed Hα and Hβ emission line flux ratios and, the electron temperature, t_e, is given in units of 10⁴ K. For the calculation of Neutral Hydrogen column density, the relation from Predehl & Schmitt (1995) was used

$$N(H I) = 5.4 \times 10^{21} \times E(B - V) \quad (3)$$

The values calculated above for the spectrum of No.1 observations of SNR Candidate ID5 together with their parameters, the relative line fluxes, the electron density N_e (calculated with The Space Telescope Science Data Analysis System (STSDAS) task nebular.temden. program; this task is based on the program FIVEL (De Robertis, Dufour & Hunt 1987; Shaw & Dufour 1995) for a five level atom) derived from the [S II](λ6716/λ6731) ratio for an assumed electron temperature 10⁴ K (Osterbrock & Ferland 2006) are shown in Table 4.

2.3 X-ray Observation and Data Reduction

We have analysed the ~97 ks *Chandra* X-ray Observatory Advanced CCD Imaging Spectrometer array (ACIS-S3) archival data of the galaxy NGC 1569 (ObsID: 782; PI: C. L. Martin) observed on 2000 April 11. The observation was telemetered in FAINT Data Mode. The data of this observation were reprocessed from Level 1 to Level 2, and analysed with *Chandra* X-ray Center (CXC) CIAO 4.9² package to remove pixel randomisation and to correct for CCD charge-transfer inefficiencies, and CALDB 4.7.6 was used for

² <http://cxc.cfa.harvard.edu/ciao/>

Table 2. Combined (No.1 and No.2) optical observations: The interference filter characteristics and our exposure times of imaging observations.

Filter	Wavelength (Å)	FWHM (Å)	Exposure times (s)	Obs. date
H α	6563	80	3 \times 300 6 \times 900	2017/03/28-29 2017/12/25
H α cont.	6446	123	1 \times 300 6 \times 300	2017/03/28-29 2017/12/25
[S II]	6728	54	3 \times 300 6 \times 900	2017/03/28-29 2017/12/25
[S II] cont.	6964	350	1 \times 300 6 \times 300	2017/03/28-29 2017/12/25

Table 3. Combined optical observations with a total of 13 SNR candidates near the central part of NGC 1569 with H α flux sensitivity; appropriate [S II]/H α ratios and their errors in parenthesis. IDs(*) indicates the possible SNR candidates coincident with those reported in radio by [Chomiuk & Wilcots \(2009\)](#) and IDs(+) indicate the possible SNR candidates, coincident with those reported in radio by [Greve et al. \(2002\)](#).

ID	RA(J2000) (h m s)	Dec. (J2000) (° ' ")	[S II] / H α	I (H α) $\times 10^{-15}$ (erg cm $^{-2}$ s $^{-1}$)
1*	04 ^h 30 ^m 47 ^s .48	64°50'55".70	0.82 (± 0.1)	6.4
2*	04 ^h 30 ^m 47 ^s .73	64°51'09".70	0.56 (± 0.1)	7.2
3*	04 ^h 30 ^m 47 ^s .91	64°50'50".30	0.64 (± 0.2)	3.7
4*	04 ^h 30 ^m 48 ^s .20	64°50'54".70	0.58 (± 0.1)	10
5*	04 ^h 30 ^m 48 ^s .42	64°50'53".60	0.46 (± 0.2)	24
6*	04 ^h 30 ^m 48 ^s .48	64°51'08".50	0.62 (± 0.1)	6.5
7 ^{*+}	04 ^h 30 ^m 49 ^s .50	64°50'59".40	0.56 (± 0.1)	7.1
8	04 ^h 30 ^m 51 ^s .24	64°50'51".05	0.50 (± 0.1)	6.1
9*	04 ^h 30 ^m 52 ^s .19	64°50'54".80	0.68 (± 0.1)	31
10	04 ^h 30 ^m 52 ^s .51	64°50'43".86	0.53 (± 0.1)	2.4
11	04 ^h 30 ^m 53 ^s .55	64°50'48".68	0.78 (± 0.1)	2.3
12*	04 ^h 30 ^m 54 ^s .08	64°50'43".50	0.57 (± 0.2)	7.5
13*	04 ^h 30 ^m 44 ^s .35	64°51'20".01	0.51 (± 0.2)	6.3

Table 4. Relative line intensity and the parameters obtained from the spectrum of the SNR candidate ID5. Fluxes are normalised F(H α) = 100. The signal-to-noise ratio are represent in parentheses beside their values and the errors of the emission line ratios and other parameters are calculated through standard error calculation.

Lines (Å)	Flux (S/N) F(H α =100)	Parameters & Line Ratios	Values
H β (λ 4861)	14.58 (4)	I (H α) (erg cm $^{-2}$ s $^{-1}$)	(2.57 \pm 0.01) $\times 10^{-14}$
[O III] (λ 4959)	19.68 (7)	[S II] ^a /H α	0.46 \pm 0.01
[O III] (λ 5007)	65.60 (18)	[S II] λ 6716/ λ 6731	1.30 \pm 0.03
[N II] (λ 6548)	6.39 (6)	[O III] (λ 5007)/H β (λ 4861)	4.5 \pm 0.07
H α (λ 6563)	100 (32)	V $_s$ (km s $^{-1}$)	100 - 150
[N II] (λ 6584)	6.75 (7)	E(B-V)	0.36 \pm 0.01
[S II] (λ 6716)	26.11 (4)	A _(Hα)	1.99 \pm 0.03
[S II] (λ 6731)	20.10 (3)	N(H I)(cm $^{-2}$)	(0.19 \pm 0.02) $\times 10^{22}$
		N $_e$ (cm $^{-3}$)	121 \pm 17

^a[S II] is the combination of λ 6716 and λ 6731 flux values.

the most recent calibration products. Spectral analysis was performed with XSPEC ([Arnaud 1996](#)) version 12.9.1³ with AtomDB v3.0.9⁴ ([Smith et al. 2001](#); [Foster et al. 2012](#)). In

this study, we selected only those data in the energy range from 0.5 to 2 keV for the soft band emission, and 0.5 to 7 keV for the full band emission to have lower particle background and lower chip quantum efficiency contamination.

³ <https://heasarc.gsfc.nasa.gov/docs/xanadu/xspec/index.html>

⁴ <http://www.atomdb.org>

2.4 X-ray Spectral Analysis

SNR candidates in our sample have low surface-brightness as being extended sources in the X-ray band. Therefore, background modelling is required to obtain meaningful information from the source. As it is the matter of the background estimation, different responses and background contributions may be associated to different regions. As a first step, in order to estimate the astrophysical background emission, the background spectra were taken from a nearby region for each source. But this method resulted in a loss in the statistical quality of the source spectra. Alternatively, selecting from a nearby emission-free circular region (centered at RA(J2000) = 04^h30^m39^s, Dec. (J2000) = 64°54′37″, with a radius of 74.46 arcsec), we defined a physically motivated background spectrum. We modelled it with various thermal and non-thermal spectral components (such as APEC and POWER-LAW) and simulated it using FAKEIT command under the XSPEC, and then, subtracted this simulated background spectrum from the source spectrum. In this observation, the Cosmic X-ray Background (CXB) and the Galactic Foreground Emission (GFE) are considered as X-ray background components. Note that, as we did not select the X-ray background emission in line of sight of the host galaxy, the foreground emission is only associated with the Milky Way, not with the host galaxy, nor with their emission combination of the galaxies. As mentioned before, we did not select an individual nearby background region for each point source spectrum since doing it this way it resulted in a loss in the statistical quality of the spectra. Otherwise, the total foreground emission would be associated with both the Milky Way and the host galaxy. CXB was modelled with an absorbed power-law spectrum, with a photon index fixed at $\Gamma = 1.46$ (Chen, Fabian & Gendreau 1997). The normalisation is the free parameter because of the non-uniformity of this component (Maggi et al. 2016). The GFE has generally small or no absorption (in our analysis it has yielded no absorption value) and modelled with APEC model, which gave an kT_e value of ~ 0.24 keV (Ryu et al. 2009). Aforementioned simulated background spectrum based on the background model, was normalised for the source region and subtracted from the spectra of the sources during the individual fitting process.

In the fitting process, the spectral models of the sources were coupled with the photoelectric absorption model (PHABS) to account for the total column density by Galactic + intergalactic + host galaxy. This value, N_H , was fixed at $0.19 \times 10^{22} \text{ cm}^{-2}$, adapted from our calculation of Neutral Hydrogen column density mean value obtained from our optical observation (see Section 2.2, Eq. 3).

As a next step, we extracted the spectra of the circular region of each SNR candidates (3.5 arcsec in radius). We grouped the spectra with a minimum of 3 counts bin^{-1} . The more appropriate method in the case of the small number of counts than χ^2 is modelling the spectral regions in order to allow the use of the Cash maximum likelihood statistic (Cash 1979). Also, all sources in this study are considered as point-like (3.5 arcsec, see Fig. 3).

In each spectral analysis, using the photoelectric absorption model of PHABS (Balucinska-Church & Mc-

Cammon 1992; Ott 2005) to account for the total column density, and setting the elemental abundances to the values measured by Anders & Grevesse (1989), we first tried to fit the spectra with a single-component Collisional Ionization Equilibrium (CIE) model APEC or variable-abundance CIE model VAPEC to search for a visual inspection for evidence of line emission. According to the residuals and goodness-of-fit, we thawed the elemental abundances or switched to non-equilibrium ionisation (NEI) models VNEI or VPSHOCK in XSPEC. In line with the feature of each model, the free parameters were the normalisation, the absorption (N_H), the electron temperature (kT_e), and the ionisation timescale ($\tau = n_e t$, where n_e , and t represent the mean electron density, and the elapsed time after the shock heating of the plasma to a constant temperature kT_e , respectively). The SNR candidates of ID4, ID5 and ID9 also have harder components to their spectra as showing emission above 5 keV, thus, we also tried to fit the spectra that show no line feature with POWER-LAW model in XSPEC to search for the non-thermal emission components, but their statistically unacceptable fits (C-stat/d.o.f > 1.5) yielded to conclusion that the thermal model is more likely to be correct. We also tried to fit with two-temperature NEI or CIE models, and obtained no statistical improvement on the fits because of the insufficient count rates from the sources. Thus, signatures of two-temperature component of NEI or CIE cannot be attained in the terms of a statistically significant improvement, neither in the goodness-of-fit, nor in the residuals. On the other hand, most of the SNR candidates have soft spectrum in the 0.5–2 keV band, and almost show no significant emission features above 2 keV. Thus, we evaluated their spectra through their proportional contribution in the soft (0.5–2 keV) and full (0.5–7 keV) energy bands with the best-fitting values.

As the ionisation ages τ in the samples were poorly constrained or high, using a NEI model did not result in a statistically significant improvement in the fits, thus, fitting with a CIE model was sufficient. Herewith, assuming APEC model based on the quality of the fit is a more preferable way for a general approach, as most of the candidates are too faint to distinguish between CIE and NEI. Amongst the SNR candidates, three of them did not require or allow elemental abundances to be fitted, neither in the soft band, nor in the full band. This could be due to insufficient data, which retain the use of free abundances in the fits. Besides, we tried to fit the SNR candidates of ID2, ID7 and ID8 with both thermal and non-thermal models, but we could not get acceptable fits with unrealistic best-fitting parameters. Hence, these sources are denoted as unclassified. The spectral results and count rates can be seen in Table 5 and individual spectra are displayed in Fig. 4. Using XSPEC, the count rates were determined from each individual source by extracting the background. We calculated the uncertainties at the 90 per cent confidence level with the ERROR command of XSPEC.

We obtained the unabsorbed X-ray fluxes and luminosities in related bands from the best-fitting models (Table 6) with the XSPEC command FLUX. Using the distance to NGC 1569 (3.4 Mpc; Kobulnicky & Skillman 1997; Jackson, Hunter & Oh 2011; Lelli, Verheijen & Fraternali 2014), we estimated the luminosity directly by our observed

unabsorbed flux values, because of the relative certainty of the SNR candidates distances.

3 DISCUSSION

3.1 Optical imaging and spectral results

In this work, the imaging and spectroscopic observations of NGC 1569 are obtained in optical band by using RTT150 telescope.

This research is based on the criteria of $[S\ II]/H\alpha \geq 0.4$, as suggested by Blair & Long (1997); Mathewson & Clarke (1973); Dopita (1997), which is used for 13 SNR candidates in NGC 1569. These 13 SNR candidates with appropriate $[S\ II]/H\alpha$ ratios and their errors are presented in Table 3.

Chomiuk & Wilcots (2009) reported their work in radio band and categorized SNR candidates in NGC 1569 by using spectral indices and $H\alpha$ images. 23 SNR candidates were reported in their work for NGC 1569 at its central region. In this work, out of 13 SNR candidates reported here, 8 of them (i.e. with ID1, 2, 3, 4, 5, 6, 7, 9, 12, 13 see Table 3) were found to be consistent with Chomiuk & Wilcots (2009) results.

The SNR candidate with ID7 shown in our Table 3, is also reported by Greve et al. (2002). Throughout NGC 1569 they reported 4 to 5 SNe and/or SNRs, located within an area of approximately 300 pc diameter around their super star clusters A, B, C where active star formation occurred until recently, and might still be going on.

In order to check the photometry calibration, $H\alpha$ fluxes of our 13 SNR candidates were compared as shown in Table 3 and marked if they were earlier detected ones, as mentioned before. $H\alpha$ flux values are found to be around $(2.2\text{--}32) \times 10^{-15} \text{ erg cm}^{-2} \text{ s}^{-1}$.

Only the spectrum of SNR candidate ID5 observations was available for analysis in this work; since the observations were done only for ID5, because of limited seeing conditions during observations, as mentioned in the previous section. This SNR candidate with ID5 here, corresponds to the coordinates given by Chomiuk & Wilcots (2009) at $(RA(J2000) = 04^h30^m48^s.42, Dec. (J2000) = 64^\circ50'53''.60)$ which is in a good agreement with ours. ID5's spectrum was obtained with the low-resolution RTT150 TFOSC. The observed emission line spectrum of the SNR candidates contains typical permitted lines of $H\alpha$, $H\beta$ and forbidden lines regions where electron density is low, this ratio should be approximately 1.5, as was pointed out by Frank, King & Raine (2002). In this study, this value is found to be 1.3 which corresponds to the electron density value, N_e , of about $121 \pm 17 \text{ cm}^{-3}$ (Table 4).

Following the work done by Dopita et al. (1984) and their Fig5. and Fig.6, the shock wave velocity, V_s , is estimated from their $[O\ III]\lambda 5007/H\beta$ line ratio diagnostics. Our optical value of $([O\ III]\lambda 5007/H\beta) = 4.5$ is in a very good agreement with their estimate of $100 < V_s < 150 \text{ km s}^{-1}$. The hydrogen column density of the SNR candidate ID5 was found to be $(0.19 \pm 0.02) \times 10^{22} \text{ cm}^{-2}$.

3.2 X-ray properties of the optically selected SNR candidates

We examined the X-ray properties of the optically detected possible SNR candidates in this work, using the thermal plasma models to search for evidence of the thermal emission, since most SNR candidates are extended sources at X-ray wavelengths, and their spectra are dominated by emission from a hot plasma. Non-thermal X-ray emission is not required to describe the observed X-ray spectrum for the 13 possible SNR candidates. Out of the 13 sources, only 10 of them have been suggested to be possible SNR candidates based on their thermal X-ray spectra, and the remaining three are denoted as unclassified because of their unacceptable fit parameters. We detected low elemental abundances in seven sources listed in Table 5. Based on their spectra, we measure the unabsorbed fluxes with a range of $(0.58 \lesssim F_X \lesssim 58.43) \times 10^{-15} \text{ erg cm}^{-2} \text{ s}^{-1}$, and the unabsorbed luminosities with a range of $(0.80 \lesssim L_X \lesssim 80.51) \times 10^{36} \text{ erg s}^{-1}$ for 10 X-ray sources. As seen in Table 6, the SNR candidates ID3 and ID5 have very high luminosity values compared with the others. The faintest source is SNR candidate ID13, which is located at the outer rim of NGC 1569. Since most of the candidates are too faint to distinguish between CIE and NEI, even the brightest sources SNR candidates ID3 and ID5, assuming CIE model APEC is a more preferable way for a general approach to understand the conditions of the plasma. The spectral analysis revealed that spectra of the SNR candidates are best modelled with the CIE plasma model with a temperature range of $0.84 \text{ keV} \lesssim kT_e \lesssim 1.36 \text{ keV}$, since the soft spectrum with $kT_e \leq 2 \text{ keV}$, which is a characteristic of the thermal SNRs, and this situation limits the possibility that they are background sources (e.g., active galactic nuclei) as indicated by Leonidaki, Zezas & Boumis (2010). Similarly, the best-fitting spectral parameters with the large errors and having small number of counts point out the fact that the considered sources might be an SNR (Leonidaki, Zezas & Boumis 2010).

Sánchez-Cruces et al. (2015) have reported 54 possible X-ray source coordinates as shown in their Table 9. They listed 54 of them with their possible description of their characteristic types that they considered as active galactic nuclei, X-ray sources, X-ray binaries, stars and two SNR candidates. On the other hand, when we have compared our coordinates originated from our optical and X-ray data analysis results for the possible SNR candidates reported here, in our work and also the radio observations reported by Chomiuk & Wilcots (2009) any of their two possible SNR candidates did not match.

4 CONCLUSIONS

In this work, our aim is to search for the possible SNR candidates in optical and X-ray wavelengths in NGC 1569. Therefore, our conclusions are as follows:

- (i) An optical imaging survey of SNR candidates in NGC 1569 is presented with the help of RTT150 observations for the first time using the $[S\ II]/H\alpha$ technique on the optical narrowband images. This search is realised for possible SNR candidates in the nearby galaxy NGC 1569 by using the criteria of $[S\ II]/H\alpha$ ratio is ≥ 0.4 as mentioned earlier. Based

Table 5. X-ray spectral results of NGC 1569 SNR candidates.

SNR Cand. ID	X-ray Count rate ($\times 10^{-4}$ count s^{-1})	kT_e (keV)	Abundances (10^{-2})	norm (10^{-5} cm $^{-5}$)	C-stat/d.o.f
1 ^a	11.85 \pm 1.14	0.98 \pm 0.17	(1)	0.11 \pm 0.03	14.53/16
3 ^a	163.50 \pm 4.12	1.09 \pm 0.12	3.47 \pm 0.03	17.67 ^{+3.89} _{-2.73}	110.06/104
4 ^b	26.62 \pm 1.68	0.95 \pm 0.15	5.03 ^{+0.04} _{-0.08}	2.48 ^{+0.71} _{-0.58}	39.94/48
5 ^b	89.12 \pm 3.05	1.07 ^{+0.13} _{-0.08}	3.24 ^{+0.03} _{-0.02}	9.39 ^{+1.37} _{-1.44}	105.42/103
6 ^a	11.33 \pm 1.12	0.91 ^{+0.99} _{-0.26}	5.23 \pm 0.27	0.66 ^{+0.45} _{-0.31}	10.32/13
9 ^b	4.43 \pm 0.72	1.36 ^{+0.82} _{-0.68}	3.48 \pm 0.13	0.58 ^{+0.72} _{-0.32}	10.72/12
10 ^a	12.36 \pm 1.16	1.18 ^{+0.68} _{-0.33}	2.22 \pm 0.28	0.91 ^{+0.41} _{-0.26}	23.63/24
11 ^a	3.94 \pm 0.69	0.84 ^{+0.44} _{-0.28}	4.69 \pm 0.19	0.44 ^{+0.53} _{-0.32}	7.19/7
12 ^a	10.92 \pm 1.10	1.18 \pm 0.18	(1)	0.12 \pm 0.05	13.75/12
13 ^a	9.06 \pm 1.01	1.04 ^{+0.48} _{-0.33}	(1)	0.05 \pm 0.03	5.46/7

Note: The normalisation, $\text{norm} = 10^{-14} \int n_e n_H dV / (4\pi d^2)$ (cm $^{-5}$), where n_e , n_H , V and d are the electron and hydrogen densities (cm $^{-3}$), emitting volume (cm 3) and distance to the source (cm), respectively. ^a: 0.5–2 keV, ^b: 0.5–7 keV energy band. (1) indicates that the elemental abundance was fixed at solar.

Table 6. Unabsorbed X-ray fluxes and luminosity values of NGC 1569 SNR candidates, considering the distance of 3.4 Mpc (Lelli, Verheijen & Fraternali 2014; Jackson, Hunter & Oh 2011; Kobulnicky & Skillman 1997).

SNR Cand. ID	F_X (10^{-15} erg cm $^{-2}$ s $^{-1}$)	L_X (10^{36} erg s $^{-1}$)
1 ^a	1.55 ^{+0.50} _{-0.30}	2.14 ^{+0.69} _{-0.41}
3 ^a	58.34 \pm 6.31	80.51 \pm 8.71
4 ^b	7.80 ^{+0.94} _{-1.48}	10.76 ^{+1.30} _{-2.04}
5 ^b	30.88 ^{+1.70} _{-2.88}	42.61 ^{+2.35} _{-3.67}
6 ^a	1.62 ^{+0.35} _{-0.61}	2.24 ^{+0.48} _{-0.84}
9 ^b	2.70 ^{+0.89} _{-1.67}	3.73 ^{+1.23} _{-2.30}
10 ^a	2.15 ^{+0.80} _{-1.34}	2.97 ^{+1.10} _{-1.85}
11 ^a	1.06 ^{+0.34} _{-0.70}	1.46 ^{+0.47} _{-0.97}
12 ^a	1.06 ^{+0.41} _{-0.81}	1.46 ^{+0.56} _{-1.12}
13 ^a	0.58 \pm 0.25	0.80 \pm 0.34

^a: 0.5–2 keV, ^b: 0.5–7 keV energy band.

on optical narrowband [S II] and H α imaging, we identified a total 13 SNR candidates in this galaxy.

(ii) The optical spectral observations were also performed for SNR candidate-ID5 which is obtained with the RTT150 TFOSC. H α , H β , [O III] λ 4959, λ 5007, [N II] λ 6548, λ 6584 and [S II] λ 6716, λ 6731 emission lines are shown in the spectrum in Fig. 2. The observed relative line fluxes and the parameters obtained from the spectrum are [S II]/H α = 0.46 \pm 0.01, [S II](λ 6716/ λ 6731) = 1.30 \pm 0.03, shock wave velocity of 100 < V_s < 150 km s $^{-1}$ (with [O III] λ 5007/H β), optical extinction E(B-V) = 0.36 \pm 0.01, $A_{(H\alpha)}$ = 1.99 \pm 0.03, absorbing column density N(H I) = (0.19 \pm 0.02) $\times 10^{22}$ cm $^{-2}$ and electron density N_e = 121 \pm 17 cm $^{-3}$ (with [S II](λ 6716/ λ 6731)).

(iii) We investigated the X-ray properties of the optically detected possible SNR candidates using *Chandra* archival

data of NGC 1569. Out of 13 sources, only 10 of them have yielded best-fit parameters with good statistics. As seen in Table 5, we measured the 0.5–2 keV and 0.5–7 keV band unabsorbed fluxes with a range of (0.58 $\lesssim F_X \lesssim 58.43$) $\times 10^{-15}$ erg cm $^{-2}$ s $^{-1}$ for 10 X-ray sources. Our spectral analysis revealed that spectra of the SNR candidates are best modelled with the CIE plasma model with a temperature range of 0.84 keV < kT_e < 1.36 keV.

ACKNOWLEDGMENTS

We are grateful to the referee for the insight and detailed comments that helped improve the manuscript. We thank TUBITAK for partial support in using RTT150 (Russian-Turkish 1.5-m telescope in Antalya) with project num-

ber 15BRTT150-842. This work is financially supported by Bogazici University, BAP through project number 8563. We thank Dr. Aytap Sezer for many useful discussions and critical reading of the manuscript and Dr. G. Branduardi-Raymont for her valuable comments.

REFERENCES

- Anders E., Grevesse N., 1989, *Geochim. Cosmochim. Acta*, 53, 197
- Arnaud K. A., 1996, *Astronomical Data Analysis Software and Systems V*, eds. G. H. Jacoby & J. Barnes, ASP Conf. Ser., 101, 17
- Balucinska-Church M., McCammon D., 1992, *ApJ*, 400, 699
- Blair W. P., Long K. S., 1997, *ApJS*, 108, 261
- Buat V., Boselli A., Gavazzi G., Bonfanti C., 2002, *A&A*, 383, 801
- Cash W., 1979, *ApJ*, 228, 939
- Chen L. W., Fabian A. C., Gendreau K. C., 1997, *MNRAS*, 285, 449
- Chomiuk L., Wilcots E.M., 2009, *AJ*, 137, 3869
- De Robertis M.M., Dufour R.J. and Hunt R.W. 1987, *JRASC*, 81, 195
- Della Ceca R., Griffiths R.E., Heckman T.M., MacKenty J.W., 1996, *ApJ*, 469, 662
- Devost D., Roy J.R., Drissen L., 1997, *ApJ*, 482, 765
- Dopita M. A., Binette L., DÓdorico S., Benvenuti P., 1984, *ApJ*, 276, 653
- Dopita M.A., 1997, *ApJ*, 485, L41
- Foster A. R., Ji L., Smith R. K., Brickhouse N. S., 2012, *ApJ*, 756, 128
- Frank J., King A., Raine D., 2002, *Accretion Power in Astrophysics*. Cambridge University Press, Cambridge, New York
- Greve A., Tarchi A., Hüttemeister S., de Grijs R., van der Hulst J. M., Garrington S. T. and Neininger N., 2002, *A&A*, 381, 825
- Grocholski A. J., Aloisi A., van der Marel R.P., Mack J., Annibali F., Angeretti L. Greggio L., Held E V., Romano D., Sirianni M., Tosi M., 2008, *ApJL*, 686, L79
- Israel, F.P. 1988, *A&A*, 194, 240
- Jackson M.C., Hunter D., Oh S., LITTLE THINGS Team, 2011, *Bull. American Astron. Soc.*, 43, 328.03
- Jacoby G. H., Africano J. L., Quigley R. J., 1987, *ASP Publications*, 99, 672
- Jürgen O., Fabian W., Elias B., 2005, *MNRAS*, 358, 1423
- Kalberla P. M. W., Burton W. B., Hartmann Dap., et al., 2005, *A&A*, 440, 775
- Kobulnicky H.A., Skillman E.D., 1997, *ApJ*, 489, 636
- Lee J. H., Lee M. G., 2014, *ApJ*, 786, 130
- Lelli F., Verheijen M., Fraternali F., 2014, *A&A*, 566, A71
- Leonidaki I., Zezas A., Boumis P., 2010, *ApJ*, 725, 842
- Long K. S., 1985, *Space Sci. Rev.*, 40, 531
- Maggi P., Haberl F., Kavanagh P. J. et al., 2016, *A&A*, 585, 162
- Massey P., Strobel K., Barnes J. V., Anderson E., 1988, *ApJ*, 328, 315
- Mathewson D. S., Clarke J. N., 1973, *ApJ*, 180, 725
- Matonick D. M., Fesen, R. A., 1997, *ApJS*, 112, 49
- Osterbrock D. E., Ferland G. J., 2006, in Osterbrock D. E., Ferland G. J., eds, *Astrophysics of Gaseous Nebulae and Active Galactic Nuclei*, 2nd edn. University Science Books, Sausalito, CA
- Ott J., Walter F., Brinks E., 2005, *MNRAS*, 358, 4
- Pannuti T. G., Duric N., Lacey C. K., Goss W. M., Hoopes C. G., Walterbos R. A. M., Magnor M. A., 2000, *ApJ*, 544, 780
- Predehl P., Schmitt J. H. M. M., 1995, *A&A*, 293, 889
- Raymond J. C., 1979, *ApJS*, 39, 1
- Raymond J.C., Hester J.J., Cox D., Blair W.P., Fesen R.A., Gull T.R., 1988, *ApJSS*. 324, 869
- Relano M., Lisenfeld U., Battaner E., Vilchez J. M., Perez-Gonzalez P., 2006a, *Spitzer Conference Infrared Diagnostics of Galaxy Evolution*
- Relano M., Lisenfeld U., Vilchez J. M., Battaner E., 2006b, *A&A*, 452, 413
- Ryu S. G., Koyama K., Nobukawa M., Fukuoka R., Tsuru, T. G., 2009, *PASJ*, 61, 751
- Sánchez-Cruces M., Rosado M., Rodríguez-González A., Reyes-Iturbide J., 2015, *ApJ*, 799, 2
- Shaw R.A., Dufour R.J. 1995, *PASP*, 107, 896
- Shull J. M., McKee C. F., 1979, *ApJ*, 227, 131
- Smith R. K., Brickhouse N. S., Liedahl D. A., Raymond J. C., 2001, *ApJ*, 556, L91
- Sonbaş E., Akyüz A., Balman Ş, Özel M. E., 2010, *A&A*, 517, A91

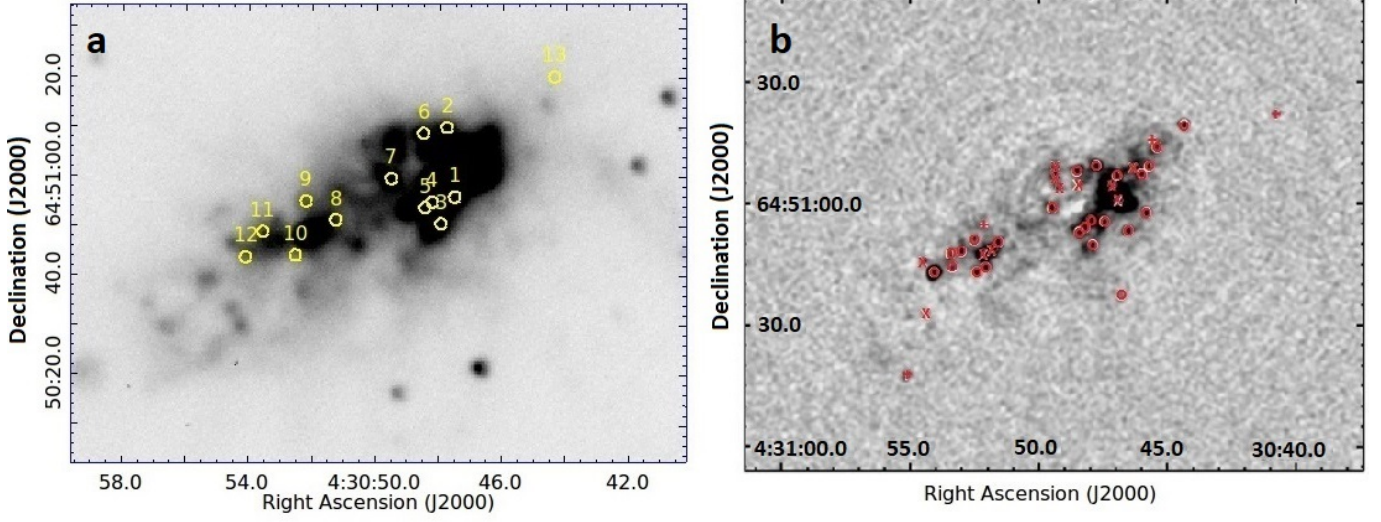


Figure 1. (a): Optical Combined Data: The $H\alpha - H\alpha$ continuum image of NGC 1569 with J2000 equatorial coordinates from optical Observations. SNR candidates are marked with yellow circles and with their ID numbers (in total 13) given in Table 3. (b) from Chomiuk & Wilcots (2009) 21 cm radio map of the central region of NGC 1569, labeled with J2000 equatorial coordinates. Here, + signs indicate background galaxies, circles are their SNR candidates, x signs are their H II regions, and * signs are sources which may be H II regions or SNR candidates. Seven sources fall outside the bounds presumed to be all classified as background galaxies.

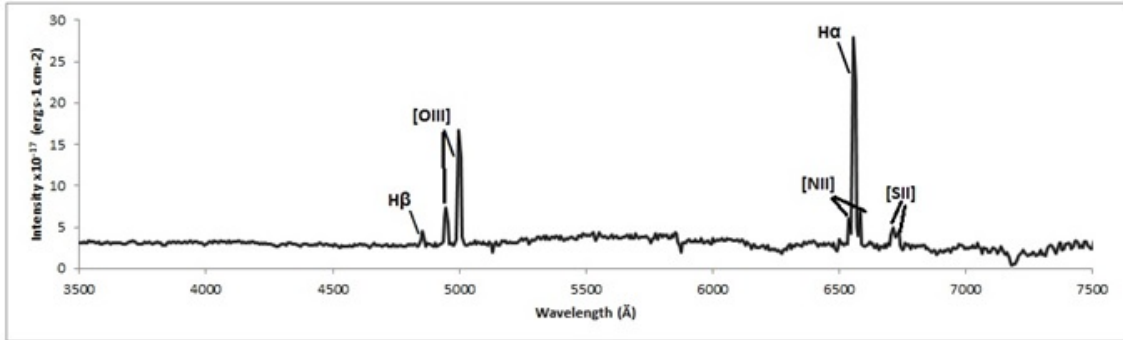


Figure 2. Optical spectrum of SNR candidate ID5; at a range of λ 3500-7500 Å at RA(J2000) = $04^{\text{h}}30^{\text{m}}48^{\text{s}}.42$, Dec. (J2000) = $64^{\circ}50'53''.60$. The Balmer $H\alpha$ λ 6563Å, $H\beta$ λ 4861Å and forbidden lines [OIII] λ 4959,5007Å, [NII] λ 6548,6584Å, [SII] λ 6717,6731Å can be seen in the spectrum.

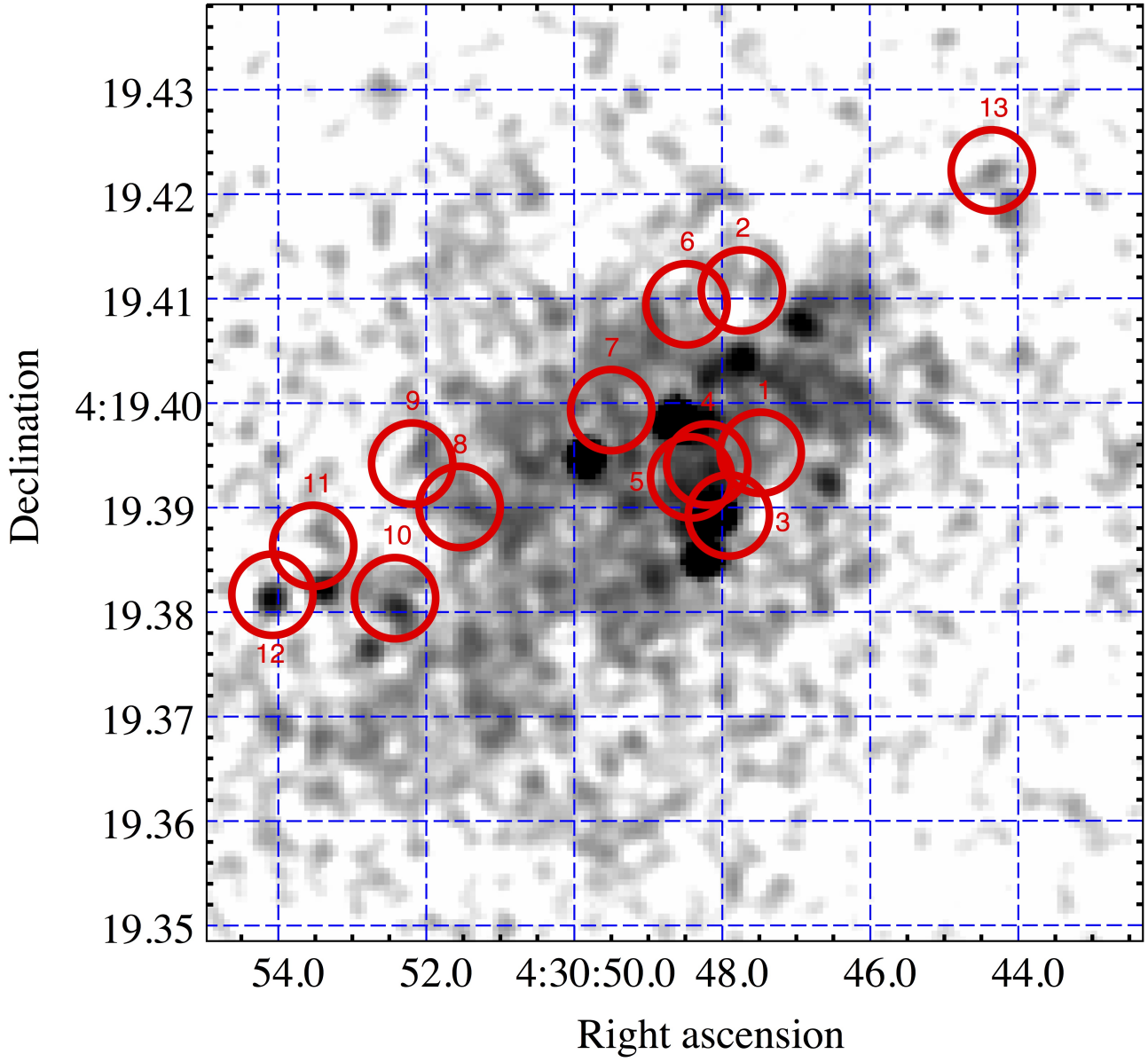


Figure 3. Exposure corrected *Chandra* ACIS-S3 image of NGC 1569 in the 0.5–7.0 keV energy band. The numbered circles indicate the extracted regions for the spectral analysis.

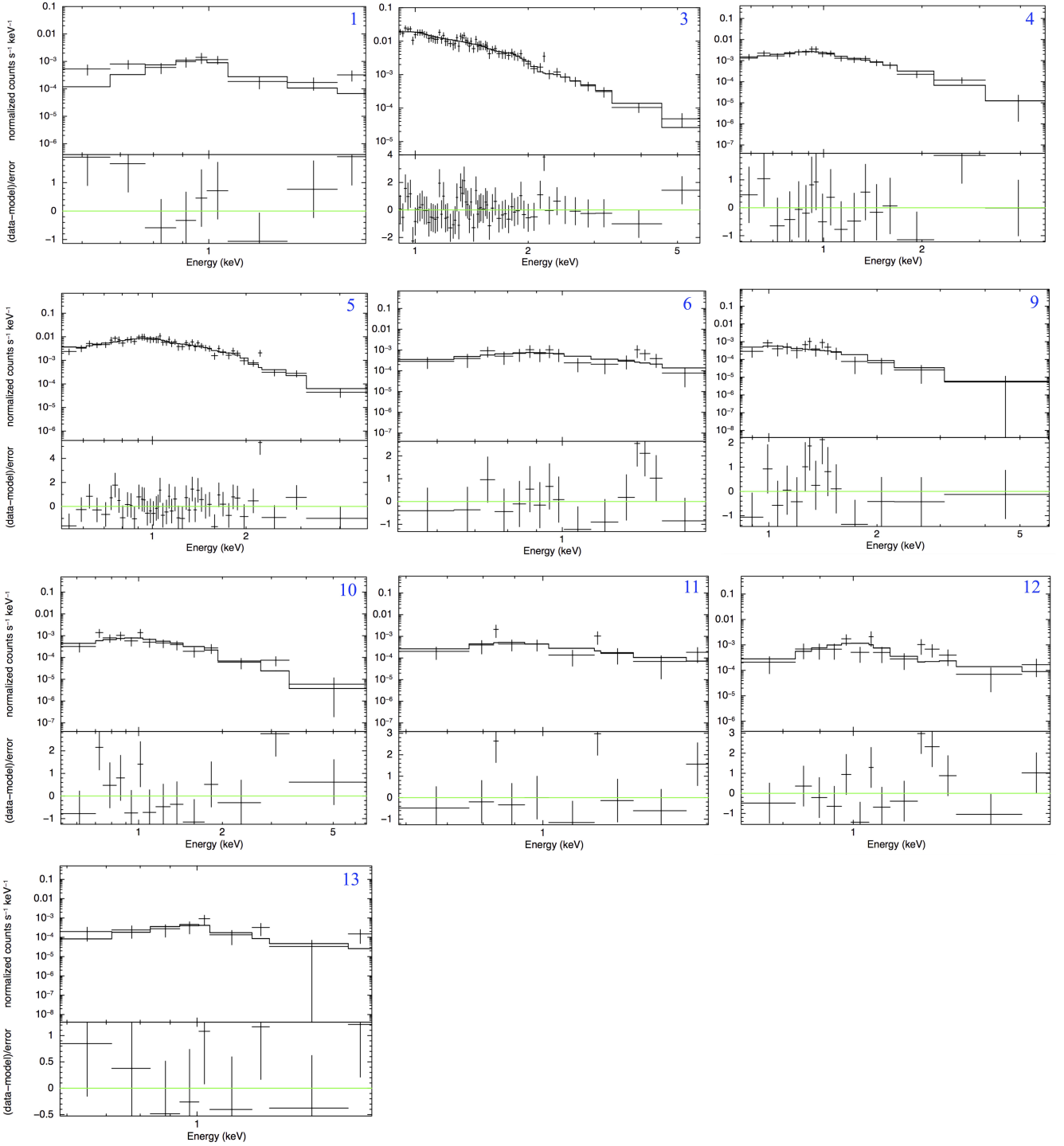


Figure 4. Background-subtracted ACIS spectra of NGC 1569 SNR candidates in the 0.5–2.0 and 0.5–7.0 keV energy bands, extracted from the point-like source regions, overlaid with the best-fitting model. The lower panels show the residuals. The spectral fitting results are summarised in Table 5.

This paper has been typeset from a $\text{T}_{\text{E}}\text{X}/\text{L}^{\text{A}}\text{T}_{\text{E}}\text{X}$ file prepared by the author.